

Comparisons of two- and three-dimensional time-dependent Hartree-Fock calculations of the reactions $^{16}\text{O} + ^{16}\text{O}$ and $^{40}\text{Ca} + ^{40}\text{Ca}^\dagger$

K. T. R. Davies

Oak Ridge National Laboratory, Oak Ridge, Tennessee 37830

H. T. Feldmeier

Institut für Kernphysik, Technische Hochschule Darmstadt, Darmstadt, West Germany

H. Flocard

Division de Physique Théorique, Institut de Physique Nucléaire B.P. No. 1, 91406 Orsay, France

M. S. Weiss

Lawrence Livermore Laboratory, University of California, Livermore, California 94550

(Received 21 June 1978)

Two-dimensional and three-dimensional time-dependent Hartree-Fock calculations have been performed over a wide range of angular momenta for $^{16}\text{O} + ^{16}\text{O}$ at $E_{\text{lab}} = 105$ MeV and for $^{40}\text{Ca} + ^{40}\text{Ca}$ at $E_{\text{lab}} = 192$ MeV. In all of the two-dimensional calculations it is assumed that the nuclear system is axially-symmetric about the line joining the mass centers of the colliding ions. Two very different two-dimensional, axially-symmetric models are considered. (a) In the first case, it is assumed that after the two ions interpenetrate the moment of inertia of the system attains the rigid-body value. (b) In the second model, each single-particle wave function is assumed to be multiplied by an extra phase factor which depends upon the azimuthal angle. This model yields an irrotational fluid flow. The results of time-dependent Hartree-Fock (TDHF) calculations with both of these models are compared with each other and with three-dimensional TDHF results. It is concluded that the two-dimensional calculations reproduce reasonably well the three-dimensional results for values of the angular momentum both below and above the three-dimensional fusion window. As the laboratory bombarding energy is decreased, there is better agreement between the two- and three-dimensional calculations, including cases in which the angular momentum is within the fusion region.

[NUCLEAR REACTIONS $^{16}\text{O}(^{16}\text{O}, x)$ and $^{40}\text{Ca}(^{40}\text{Ca}, x)$ in 2- and 3-dimensional time-dependent Hartree-Fock calculations. Comparisons between 2- and 3-dimensional results. Fusion and strongly damped collisions.]

I. INTRODUCTION

Over the last few years a variety of time-dependent Hartree-Fock (TDHF) studies have been reported.¹⁻¹⁴ Most of these involve light-ion reactions which include both two-dimensional (2D)^{2,3,5,6,7,13,14} and three-dimensional (3D)^{4,9,10,11,13,14} calculations. One crucial question that needs to be answered is how well does exact TDHF relate to experiment. By exact TDHF we mean those equations derived from a variational principle with a single determinantal wave function and without further *ad hoc* assumptions.^{7,9} Some recent 3D TDHF calculations^{10,11,15} are encouraging since they show that the calculated $^{16}\text{O} + ^{16}\text{O}$ fusion cross sections are in excellent agreement with the experimental data.

One expects that TDHF with its inherent mean field approximation should be more adequate for heavy rather than light systems and at relatively low energies above the Coulomb barrier. For heavy systems 3D calculations are at present

prohibitively expensive, but studies that simulate 3D physics within the context of a 2D model are manageable and are being pursued.^{16,17} However, a prerequisite to delineate the validity of the 2D programs is a proper comparison with 3D results. Some such comparisons have already been made.^{11,13,14,18} The purpose of this paper is to offer a detailed intercomparison between various *axially-symmetric* 2D models and accurate 3D calculations, with particular emphasis on understanding how valid the 2D models are for calculations of very heavy-ion reactions.

In Sec. II of this paper we discuss two completely different two-dimensional models. Both assume that the *densities* of the colliding nuclei remain axially symmetric about the rotating line joining their mass centers.^{2,6,7} In the first model an assumption is made about the moment of inertia, which becomes discontinuous when the two ions "clutch."^{2,6,7} Clutching occurs when the two ions just begin to strongly interpenetrate one another, so that the density at the center of the system ex-

ceeds some critical value. One assumes that before clutching the moment of inertia is that of two separated point masses, while after clutching it is given by the *rigid-body* value. We also discuss several variations of this model which are significant improvements over the original version used in previous calculations.^{2,6,7}

In the second model, each single-particle wave function is multiplied by an additional phase function which depends in a nontrivial way on the azimuthal angle.¹² Additional variation of this phase function yields a differential equation coupling it to the density. All quantities of physical interest, such as the orbital angular momentum, the rotational energy or the moment of inertia are obtained by calculating expectation values of the corresponding operators. Thus, effects from the Coriolis term $\vec{\omega} \cdot \vec{L}$ or the rotational part of the kinetic energy $\vec{L}^2/2\mathcal{G}$ are taken into account in a natural way. This model has the appealing feature of being completely self-consistent, with both the single-particle wave functions and the phase function being determined from a variational principle.¹² If the same phase function is used for all single-particle wave functions, then the model gives an *irrotational* moment of inertia.^{19,20}

In Sec. III we present TDHF results from the various axially-symmetric 2D models for the reactions $^{16}\text{O} + ^{16}\text{O}$ at $E_{\text{lab}} = 105$ MeV and $^{40}\text{Ca} + ^{40}\text{Ca}$ at $E_{\text{lab}} = 192$ MeV. These results are compared with those obtained from exact 3D calculations.¹⁰ In order to ascertain the validity of 2D TDHF for a very heavy system, we picked the $^{40}\text{Ca} + ^{40}\text{Ca}$ laboratory bombarding energy according to the following prescription. This energy, $E_{\text{lab}} = 192$ MeV, gives a relative velocity above the Coulomb barrier which is equal to the corresponding velocity for the $^{84}\text{Kr} + ^{209}\text{Bi}$ system at $E_{\text{lab}} = 600$ MeV.²¹ Thus, we feel that the $^{40}\text{Ca} + ^{40}\text{Ca}$ comparisons give some measure of the validity of the axially-symmetric 2D models for calculations of the scattering of heavier ions.

Finally in Sec. IV of this paper we summarize our conclusions.

II. AXIALLY-SYMMETRIC, TWO-DIMENSIONAL TDHF MODELS

A. Rigid-body moment-of-inertia (clutching) model

The basic model, which we denote as R1, has been thoroughly discussed in previous references,^{2,6,7} which give details regarding computation of the total energy, the single-particle potential, and the rigid-body moment of inertia. The main features of this model, are described as follows. The TDHF calculation is performed in

two nontrivial dimensions, assuming that the colliding nuclei remain axially symmetric about the rotating line joining their mass centers. We assume an ansatz for the moment of inertia. When the two ions are far apart (both before "clutching" and after "declutching"), the moment of inertia $\mathcal{G}[\rho]$ is assumed to be that of two point masses

$$\mathcal{G}[\rho] = \mu R^2, \quad \rho_0(t) < \rho_c, \quad (1)$$

where μ is the reduced mass of the system, R is the separation coordinate^{2,6,7} of the two ions, $\rho_0(t)$ is the (time-dependent) density at the center of mass, and ρ_c is a (constant) clutching density. The notation $\mathcal{G}[\rho]$ indicates that \mathcal{G} is a functional of the density.⁶ When ρ_0 exceeds ρ_c , the nuclei are assumed to have "clutched" and the moment of inertia is taken to be that of a rigid body

$$\mathcal{G}[\rho] = \mathcal{G}_R[\rho], \quad \rho_0(t) \geq \rho_c, \quad (2)$$

where $\mathcal{G}_R[\rho]$ is the rigid-body value. We take $\rho_c = 0.07 \text{ fm}^{-3}$, which is approximately one half of the saturation density of nuclear matter for the effective interaction¹ used in our calculations.

The rate of rotation of the symmetry axis is given by

$$\omega = \frac{d\theta}{dt} = \frac{L_{\text{tot}}}{\mathcal{G}[\rho]}, \quad (3)$$

where L_{tot} is the conserved *total* angular momentum along the rotation axis perpendicular to the scattering plane. The final center-of-mass scattering angle $\theta_{\text{c.m.}}^{(f)}$ and the asymptotic value of the total center-of-mass translational kinetic energy $E_{\text{c.m.}}^{(f)}$ are calculated by matching to a point Coulomb trajectory after the collision. In this model R1 we note that after declutching, the intrinsic angular momentum vanishes, so that L_{tot} is the exact orbital angular momentum along the asymptotic Coulomb trajectory.

The discontinuity in the moment of inertia at the time when clutching occurs results in a loss of collective energy. This energy is absorbed into internal rotational degrees of freedom which are not explicitly taken into account in the axially-symmetric model. Thus, this loss in calculated collective energy may be related to a physical process. It is not expected to feed back into collective relative motion. However, there is also a discontinuity in the moment of inertia at the time of declutching, which causes the collective energy to abruptly *increase*. This effect, we believe, is unphysical and is a major weakness of model R1.

This completes the description of the basic model R1 used in all previous rigid-body, clutching calculations.^{2,6,7} We now present three variations of this model which correct various deficiencies in R1 and can lead to significantly different values

of the final scattering angle $\theta_{\text{c.m.}}^{(f)}$ and the final kinetic energy $E_{\text{c.m.}}^{(f)}$.

Prescription R2 is the same as R1 except that $\mathcal{J}[\rho]$ remains the rigid-body value until the two systems completely separate, so that there is no discontinuity in either the moment of inertia or the rotational energy at the time when $\rho_0(t)$ becomes less than ρ_c again. Thus, one major weakness of model R1 is corrected. In this model there is nonzero intrinsic angular momentum after separation, so that it is important to compute the final scattering angle $\theta_{\text{c.m.}}^{(f)}$ and the final energy $E_{\text{c.m.}}^{(f)}$ immediately after the ions have separated, using the true orbital angular momentum

$$L_{\text{orb}} = \mu R^2 \omega, \quad (4)$$

where ω is given by Eq. (3).

Prescription R3 is the same as R1 except that after declutching [$\rho_0(t) < \rho_c$],

$$\omega = L_{\text{orb}}^{(\text{dec})} / \mu R^2, \quad (5)$$

where $L_{\text{orb}}^{(\text{dec})}$ is the orbital angular momentum just before the system has declutched. Also, $\theta_{\text{c.m.}}^{(f)}$ and $E_{\text{c.m.}}^{(f)}$ are computed using $L_{\text{orb}}^{(\text{dec})}$ for the final Coulomb trajectory. This model is very similar to R2, as we will show in the next section.

Note that prescriptions R1, R2, and R3 all give rise to exactly the same time evolution of the system before clutching occurs and during the entire period during which $\rho_0 \geq \rho_c$. The three prescriptions differ only after declutching has occurred. Thus, R1, R2, and R3 give exactly the same results for cases in which the system never separates (fusion) or if the system never clutches (peripheral scattering).

R4 is a prescription which is based on R2 but allows for a continuous change in the moment of inertia before clutching occurs. It is assumed that

$$\mathcal{J}[\rho] = \alpha(t)(\mu R^2) + \beta(t)\mathcal{J}_R[\rho], \quad (6)$$

where

$$\beta(t) \equiv \begin{cases} (4/\pi) \tan^{-1}[\rho_0(t)/\rho_c], & \text{for } \rho_0(t) < \rho_c \\ 1, & \text{for } \rho_0(t) \geq \rho_c \end{cases} \quad (7a)$$

and

$$\alpha(t) \equiv 1 - \beta(t). \quad (7b)$$

For $\rho_0 \ll \rho_c$ we see that $\mathcal{J}[\rho] \approx \mu R^2$, while for $\rho_0 \geq \rho_c$ we have $\mathcal{J}[\rho] = \mathcal{J}_R[\rho]$. After clutching occurs and for the remainder of the calculation, it is assumed that $\mathcal{J}[\rho] = \mathcal{J}_R[\rho]$. Thus, there is no sudden jump in the moment of inertia or in the rotational energy at the time of clutching. As in prescriptions R1, R2, and R3, there is a net loss of collective energy over the time period when the ions

start to overlap until they clutch. However, in contrast to the other models, this loss occurs continuously rather than suddenly at the time of clutching. In order that intrinsic rotational energy not be fed back into orbital motion, we impose the condition that β is never allowed to decrease. Thus, in the case of a peripheral collision, when no clutching occurs, β reaches a maximum value β_{max} and for the rest of the calculation, $\beta = \beta_{\text{max}}$ and $\alpha = 1 - \beta_{\text{max}}$. Also, in this prescription, $\theta_{\text{c.m.}}^{(f)}$ and $E_{\text{c.m.}}^{(f)}$ are computed using Eq. (4) with ω obtained from Eq. (3). Obviously, R4 gives different results from the other models for all L values, but the differences are expected to be especially pronounced at larger L values where fusion and orbiting occur.

B. The self-consistent phase model

It is possible to extend axial symmetry to collisions with an impact parameter not equal to zero by also allowing the wave function to have an additional phase.¹² The method will now be described briefly. A coordinate system $\{x, y, z\}$ is chosen such that the z axis is given by the line which joins the mass centers of the colliding nuclei (see Fig. 1). The total center of mass lies at the origin and the y axis is perpendicular to the reaction plane. Cylindrical coordinates $\{r, z, \phi\}$ are introduced with

$$r = (x^2 + y^2)^{1/2}, \quad \phi = \arctan \frac{y}{x}, \quad z = z.$$

For an axially symmetric system, each single-particle wave function may take the form

$$\psi_\lambda(r, z, \phi) = \hat{\psi}_\lambda(r, z) e^{i n_\lambda \phi} e^{i \chi_\lambda(r, z, \phi)}. \quad (8)$$

Here n_λ is an integer and $\chi_\lambda(r, z, \phi)$ is real, whereas $\hat{\psi}_\lambda(r, z, \phi)$ is complex. Then $|\psi_\lambda|^2$ is a function of only r and z . Since the wave function has to be continuous for $\phi = 0$ and $\phi = 2\pi$, $\chi(r, z, \phi + 2\pi)$ has to

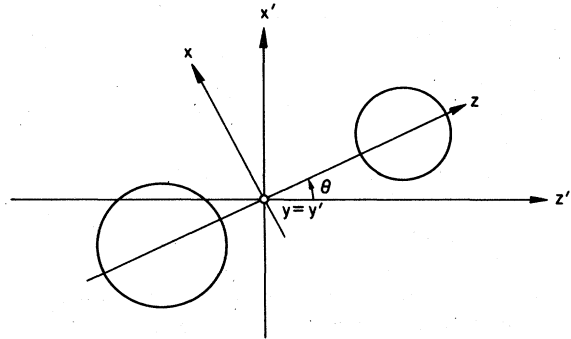


FIG. 1. Coordinate system for the rotating frame approximation.

be periodic. The most general form would be

$$\chi_\lambda(r, z, \phi) = \sum_{\kappa=1}^{\infty} [g_\lambda^{(\kappa)}(r, z) \cos \kappa \phi + f_\lambda^{(\kappa)}(r, z) \sin \kappa \phi]. \quad (9)$$

We choose χ_λ to be

$$\chi_\lambda(r, z, \phi, t) = g_\lambda(r, z, t) \cos \phi. \quad (10)$$

This allows the system the freedom to have a momentum in the x direction. With

$$p_x = \frac{\hbar}{i} \frac{\partial}{\partial x} = \frac{\hbar}{i} \left(\cos \phi \frac{\partial}{\partial r} - \frac{1}{r} \sin \phi \frac{\partial}{\partial \phi} \right), \quad (11)$$

one obtains

$$\langle \psi_\lambda | p_x | \psi_\lambda \rangle = \pi \hbar \int r dr dz |\psi_\lambda|^2 \left(\frac{\partial g_\lambda}{\partial r} + \frac{1}{r} g_\lambda \right), \quad (12)$$

where g_λ and $|\psi_\lambda|^2$ are functions of only the coordinates r and z . This can be easily understood for the following simple example:

$$\hat{\psi}_\lambda(r, z) e^{i k x} = \hat{\psi}_\lambda(r, z) e^{i k r \cos \phi},$$

for which we find that $g(r, z) = kr$ and $\langle \psi_\lambda | p_x | \psi_\lambda \rangle = \hbar k$ if $\hat{\psi}_\lambda$ is normalized to unity. The term $f_\lambda(r, z, t) \cdot \sin \phi$ would correspond to a momentum in the y -direction perpendicular to the reaction plane which is supposed to be zero.

The single-particle equations for $\hat{\psi}_\lambda$ and g_λ are obtained in the usual way by requiring that the action

$$\mathcal{Q} = \int_{t_1}^{t_2} \langle \Psi' | (i\hbar \partial / \partial t - H) | \Psi' \rangle dt \quad (13)$$

be stationary under variations. Ψ' is a Slater determinant written in the inertial frame $\{x', y', z'\}$ (see Fig. 1). This transforms into the rotated frame $\{x, y, z\}$ by

$$D_\theta \Psi' = \Psi, \quad D_\theta = e^{(i/\hbar)\theta L_y}, \quad (14)$$

$$L_y = \sum_{\lambda=1}^A (\vec{r}_\lambda \times \vec{p}_\lambda)_y.$$

Assuming H to be rotationally invariant, we obtain

$$\mathcal{Q} = \int_{t_1}^{t_2} \langle \Psi | [D_\theta i\hbar (\partial / \partial t) D_\theta^{-1} - H] | \Psi \rangle dt,$$

or from Eq. (14)

$$\mathcal{Q} = \int_{t_1}^{t_2} \langle \Psi | (i\hbar \partial / \partial t + \omega L_y - H) | \Psi \rangle dt, \quad \omega = \frac{\partial \theta}{\partial t}. \quad (15)$$

For simplicity we assume that all single-particle wave functions ψ_λ have the same phase χ , resulting in a collective kind of motion for the rotation. Due to this assumption, the Hartree-Fock potential V_{HF} used in this paper does not depend on χ .

Therefore we find that

$$\mathcal{Q} = \int_{t_1}^{t_2} \sum_\lambda \langle \psi_\lambda | \left(i\hbar \frac{\partial}{\partial t} + \hbar \vec{\omega} \cdot (\vec{r} \times \vec{\nabla}) \chi + \frac{\hbar^2}{2m} [\vec{\nabla}^2 - (\vec{\nabla} \chi)^2] - V_{\text{HF}} \right) | \psi_\lambda \rangle dt, \quad (16)$$

with

$$\psi_\lambda(r, z, \phi) = \hat{\psi}_\lambda(r, z) e^{i n_\lambda \phi}$$

and

$$\vec{\omega} = \frac{d\theta}{dt} \vec{e}_y,$$

where \vec{e}_y is a unit vector in the y direction. Terms like $\langle \psi_\lambda | (\partial / \partial t) \chi | \psi_\lambda \rangle$ and $\langle \psi_\lambda | \vec{\nabla} \chi \cdot \vec{\nabla} | \psi_\lambda \rangle$ are zero due to the integration over ϕ . Varying \mathcal{Q} with respect to $\hat{\psi}_\lambda$, we obtain the TDHF equations

$$i\hbar \frac{\partial}{\partial t} \hat{\psi}_\lambda = -\frac{\hbar^2}{2m} \left(\frac{\partial^2}{\partial r^2} + \frac{1}{r} \frac{\partial}{\partial r} + \frac{\partial^2}{\partial z^2} - \frac{n_\lambda^2}{r^2} \right) \hat{\psi}_\lambda + v_{\text{HF}} \hat{\psi}_\lambda \quad (17a)$$

$$+ \frac{\hbar^2}{2m} \frac{1}{2} \left[\left(\frac{\partial g}{\partial r} \right)^2 + \left(\frac{\partial g}{\partial z} \right)^2 + \left(\frac{g}{r} \right)^2 \right] \hat{\psi}_\lambda \quad (17b)$$

$$- \hbar \omega \frac{1}{2} \left[z \left(\frac{\partial g}{\partial r} + \frac{g}{r} \right) - r \frac{\partial g}{\partial z} \right] \hat{\psi}_\lambda. \quad (17c)$$

The first line (17a) is the same as for central collisions. The second and the third lines (17b) and (17c) represent, respectively, the rotational energy part and the Coriolis part $\vec{\omega} \cdot \vec{L}$ of the TDHF Hamiltonian. Varying \mathcal{Q} in Eq. (16) with respect to χ (i.e., with respect to g), we obtain an equation for χ

$$\frac{\hbar^2}{m} \vec{\nabla} \cdot (\rho \vec{\nabla} \chi) - \hbar \vec{\omega} \cdot (\vec{r} \times \vec{\nabla} \rho) = 0, \quad (18a)$$

or written in terms of g ,

$$\frac{\partial \rho}{\partial r} \frac{\partial g}{\partial r} + \frac{\partial \rho}{\partial z} \frac{\partial g}{\partial z} + \rho \left(\frac{\partial^2 g}{\partial r^2} + \frac{1}{r} \frac{\partial g}{\partial r} + \frac{\partial^2 g}{\partial z^2} - \frac{1}{r^2} g \right) = \frac{m\omega}{\hbar} \left(z \frac{\partial \rho}{\partial r} - r \frac{\partial \rho}{\partial z} \right). \quad (18b)$$

Equation (18) turns out to be a type of continuity equation for the additional rotating flow $\rho \vec{\nabla} \chi$ where the change in time of ρ due to the rotating frame velocity field $\vec{\omega} \times \vec{r}$ is given by

$$\frac{d\vec{r}}{dt} \cdot \vec{\nabla} \rho = (\vec{\omega} \times \vec{r}) \cdot \vec{\nabla} \rho = \vec{\omega} \cdot (\vec{r} \times \vec{\nabla} \rho).$$

Equation (18) shows that g is linear in ω . Therefore, we first solve (18b) at each time step for $\vec{g} = (1/\omega)g$. Next we find ω by calculating the conserved expectation value for L_y ,

$$L = \langle L_y \rangle = \hbar \sum_{\lambda} \langle \hat{\psi}_{\lambda} | (\vec{r} \times \vec{\nabla}_{\chi})_y | \hat{\psi}_{\lambda} \rangle, \quad (19a)$$

or

$$L = \hbar \omega \int \rho \left[z \left(\frac{\partial \vec{g}}{\partial r} + \frac{\vec{g}}{r} \right) - r \frac{\partial \vec{g}}{\partial z} \right] \pi r dr dz. \quad (19b)$$

The quantity $g = \omega \vec{g}$ is then used in the TDHF equations (17b) and (17c) for the additional rotational potentials.

Equation (19) also results in a natural definition for the moment of inertia \mathcal{I}

$$\mathcal{I} = \pi \hbar \int \rho \left[z \left(\frac{\partial \vec{g}}{\partial r} + \frac{\vec{g}}{r} \right) - r \frac{\partial \vec{g}}{\partial z} \right] r dr dz. \quad (20)$$

The rotational energy is given by

$$E_{\text{rot}} = \sum_{\lambda} \left\langle \hat{\psi}_{\lambda} \left| \frac{\hbar^2}{2m} (\vec{\nabla}_{\chi})^2 \right| \hat{\psi}_{\lambda} \right\rangle. \quad (21)$$

Using Eqs. (18)–(21), one can show that the usual relation

$$E_{\text{rot}} = \frac{L^2}{2\mathcal{I}} \quad (22)$$

is satisfied. The above approximation to the full three-dimensional picture is exact in the cases of central collisions ($L=0$) and two spherical nuclei passing each other without touching. (A more detailed discussion is given in Ref. 12.)

In the phase model we have allowed the system to have another “degree of freedom” in the form of the additional phase χ . This is the simplest possible assumption one can make in order to describe a rotation in which one obtains a nonvanishing ϕ -averaged current in the x direction ($\int j_x d\phi \neq 0$). The additional current \vec{j} due to this phase is $(\hbar/m)(\vec{\nabla}_{\chi})\rho$ with the related velocity field $\vec{v} = \vec{j}/\rho = (\hbar/m)\vec{\nabla}_{\chi}$. Since $\vec{\nabla} \times \vec{v} = 0$, it is clear that the rotation around the y axis is described by an *irrotational* velocity field. Thus, the moment of inertia \mathcal{I} given in Eq. (20) is an irrotational moment of inertia in contrast to the clutching model where we assumed the rotation of a rigid body.

We obtained irrotational flow because we assumed the same phase χ for all single-particle wave functions. The velocity field for different phases would be

$$\vec{v} = \frac{(\hbar/m) \sum_{\lambda} |\hat{\psi}_{\lambda}|^2 \vec{\nabla}_{\chi_{\lambda}}}{\sum_{\lambda} |\hat{\psi}_{\lambda}|^2}. \quad (23)$$

Here $\vec{\nabla} \times \vec{v}$ is not necessarily zero. However, different phases χ_{λ} would cause quite complicated equations, mainly because ψ_{λ} [as defined by Eq. (8)] is not orthogonal to ψ_{μ} if $\hat{\psi}_{\lambda}$ is orthogonal to

$\hat{\psi}_{\mu}$. In the simple single phase model described above both ψ_{μ} and $\hat{\psi}_{\mu}$ are sets of orthogonal functions.

III. RESULTS

The 2D models discussed in Sec. II provide us with examples of the two limiting cases of rigid-body rotation and irrotational fluid flow. We now compare results of calculations using these axially-symmetric 2D models. We also compare with exact 3D results,^{10,14} in which one expects the type of rotation to be somewhere in between that of a rigid-body and irrotational flow.

A. Calculations of $^{16}\text{O} + ^{16}\text{O}$ at $E_{\text{lab}} = 105$ MeV

The two-body potential used in all of our calculations is the zero-range, modified Skyrme interaction of Ref. 1, plus the Coulomb potential.⁶

Before comparing the two different axial approaches with 3D calculations, one has to first make sure that there are no differences in the results due to the different methods of numerically treating the TDHF equations. The main difference lies in the size of the mesh spacings. In the axial codes we use $\Delta r = \Delta z = 0.4$ fm and a three-point formula for the second derivatives in the kinetic energy.^{2,6,7} For the three-dimensional code we use $\Delta x = \Delta y = \Delta z = 1.0$ fm and a five-point formula for the second derivatives.¹⁰ Detailed information on the two different numerical approaches can be found in Refs. 6 and 10.

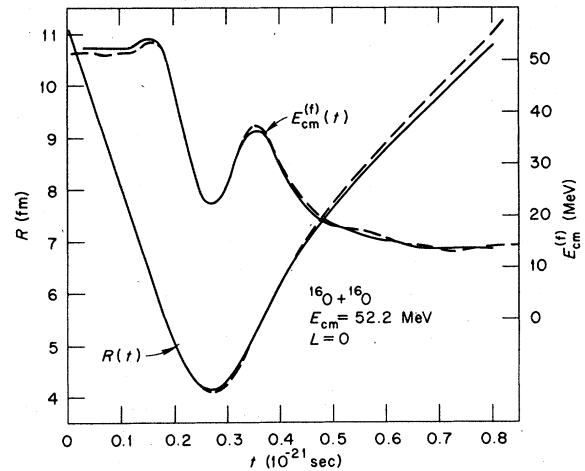


FIG. 2. The separation distance $R(t)$ in fermis and $E_{\text{c.m.}}^{(f)}(t)$ in MeV for $^{16}\text{O} + ^{16}\text{O}$ for $E_{\text{c.m.}} = 52.2$ MeV and $L = 0$. The full and dashed curves are, respectively, for 2D and 3D TDHF calculations. The initial energy of 52.2 MeV was the value actually used in the 3D calculation (see Ref. 10).

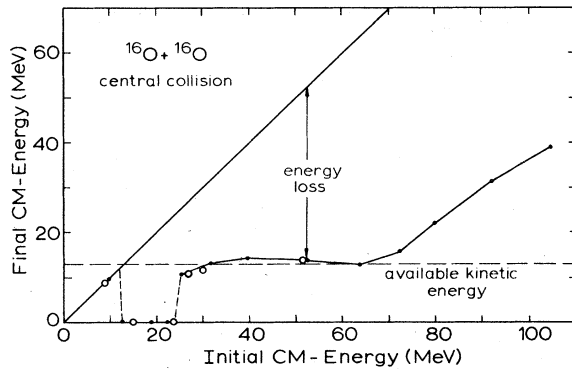


FIG. 3. Final center-of-mass energy vs initial center-of-mass energy for central collisions of $^{16}\text{O}+^{16}\text{O}$. The dark points and the open circles are results of axial 2D and 3D calculations (Ref. 10), respectively. The full line connects the 2D results.

In Fig. 2 we compare for a central collision (for which both codes should give the same results) the distance $R(t)$ of the mass centers as a function of time. The second curve shows the projected asymptotic kinetic energy of the fragments

$$E_{\text{c.m.}}^{(f)}(t) = \frac{\mu}{2} [\dot{R}(t)]^2 + \frac{Z_1 Z_2 e^2}{R(t)}.$$

At $t=0$ $E_{\text{c.m.}}^{(f)}(t)$ is the initial energy, $E_{\text{c.m.}} = 52.2$ MeV. Then the nuclear attraction sets in and increases the velocity slightly after which the energy dissipation slows down the fragments to a final energy of 14 MeV. Up to very small deviations both the 2D and the 3D codes give the same result. The same close agreement between the two codes can be seen in another comparison shown in Fig. 3 where we display the final energy for central collisions as a function of the initial energy. For low initial energies up to 9 MeV in the center-of-mass system we obtain Coulomb scattering. When the system is able to overcome the Coulomb barrier, it fuses in an initial energy range between 12 and 24 MeV. For higher energies up to about 75 MeV all of the available kinetic energy is dissipated and the final energy is the Coulomb energy of about 14 MeV, independent of the initial energy. For initial energies above 75 MeV the energy loss is less than the available energy.

Figure 4 shows a comparison of deflection function and energy loss curves for $^{16}\text{O}+^{16}\text{O}$ at $E_{\text{c.m.}} = 52.5$ MeV. The 3D calculation¹⁰ shows a fusion window between $L = 13\hbar$ and $L = 28\hbar$. At this energy the system never fuses for either the phase or the clutching model. For the axial approximation we observe only orbiting behavior. The phase model exhibits orbiting near the lower edge of the

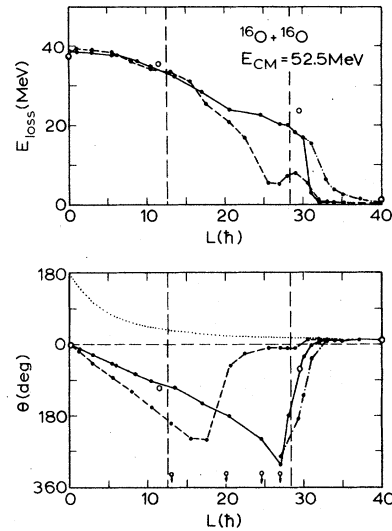


FIG. 4. Energy loss and deflection function curves for $^{16}\text{O}+^{16}\text{O}$ at $E_{\text{c.m.}} = 52.5$ MeV. The full curve connects points which are results of model R2, the dashed curve is for the phase model, the dot-dashed curve is for R4 and the open circles represent 3D results. Those 3D points having arrows pointing towards large negative angles correspond to fusion. The dotted line in the deflection function graph is for pure Coulomb scattering.

3D fusion window whereas the clutching model in either version R2 or R4 displays orbiting at the upper edge of the window.

For L values below the 3D fusion window the 3D energy-loss curve practically coincides with the one obtained by either the rigid rotation (R2) or the irrotational flow (P) assumption. In the deflection function the 3D results lie in between R2 and P.

Above the 3D fusion window the different models give different answers. The least energy is dissipated in R2 for L values higher than $31\hbar$ where the system did not clutch at all. The jump in the R2 curves between $L = 30\hbar$ and $L = 31\hbar$ reflects the differences between the clutched and nonclutched modes. About 13 MeV has to be regarded as energy dissipated into internal rotational degrees of freedom by going from $L = 30\hbar$ to $L = 31\hbar$. The self-consistent phase model allows for slightly more dissipation than R2 for $L > 30\hbar$ but its validity seems to break down at $L \approx 28\hbar$ since there is less energy loss for decreasing impact parameters. We obtain large energy losses even for only slightly grazing collisions in version R4 in which we allow a smooth transition to rigid rotation. R4 gives nearly the same results as R2 for $L \leq 30\hbar$ where the system clutches. R3 is not

TABLE I. Comparisons of $L_{\text{loss}}^{\text{orb}}$ and E_{loss} for $^{16}\text{O}+^{16}\text{O}$ at $E_{\text{c.m.}} = 52.5$ MeV.

L (\hbar)	R4			3D	
	$L_{\text{loss}}^{\text{(orb)}}$ (\hbar)	E_{loss} (MeV)	$E_{\text{loss}}^{\text{(rot)}}$ (MeV)	$L_{\text{loss}}^{\text{(orb)}}$ (\hbar)	E_{loss} (MeV)
29	5.6	18.1	8.2	5.5	23.2
30	5.9	17.1	8.6		
31	6.6	15.2	8.9		
33	2.7	6.3	3.4		
35	1.0	2.7	1.4		

shown since the results are very similar to those of R2. It is an open question whether our results can be interpreted as implying a real rigid rotation in the 3D case. In Table I the loss of orbital angular momentum $L_{\text{loss}}^{\text{(orb)}}$, of energy E_{loss} , and of rotational energy $E_{\text{loss}}^{\text{(rot)}}$, which arises from changing the moment of inertia, are given for different initial angular momenta using R4. About half of the energy is dissipated by increasing the moment of inertia. The loss in orbital angular momentum seems to be reproduced by R4, but the scattering angles are too negative.

Altogether model R2 seems to simulate a 3D calculation best. However, it should be regarded as a phenomenological recipe to account for the lack of degrees of freedom in an axial 2D approach.

These results are in close agreement to those obtained by Bonche, Grammaticos, and Koonin¹¹ in which 3D $^{40}\text{Ca}+^{40}\text{Ca}$ results for a center-of-mass energy of 139 MeV are compared with previous 2D results.⁶ Also their fusion limits for $^{16}\text{O}+^{16}\text{O}$ agree with ours shown in Fig. 3 for $L=0$.

The comparison seems to indicate that the 2D phase model reproduces somewhat better the 3D results at the lower end of the fusion window, while the 2D clutching model gives a better representation of 3D at the upper end of the window. These qualitative features of the 2D models can also be seen in the polar $R-\theta$ plots shown in Figs. 5 and 6. For $L=13\hbar$ at the lower end of the fusion window the phase model trajectory more closely follows the 3D curve up until about $\theta \approx 50^\circ$, whereas for $L=27\hbar$ at the upper end of the window it is the R2 rigid clutching trajectory which more closely follows the 3D curve for half of a full rotation. Also, Fig. 5 shows that at $L=5.5\hbar$, below the 3D fusion window, the R2 and 3D curves are almost identical.

B. Calculations of $^{40}\text{Ca}+^{40}\text{Ca}$ at $E_{\text{lab}} = 192$ MeV

The previous comparisons have been at sufficiently high energy that one expects nonaxially-symmetric deformations to be important, especially

in the fusion region.^{10,11,18} However, we know that there are lower energy cases for which one obtains significant fusion in an axially-symmetric 2D calculation.⁶ For example, in the comparison made in Sec. III A for $^{16}\text{O}+^{16}\text{O}$ at $E_{\text{lab}} = 105$ MeV, fusion does not occur for any 2D model but does occur in the 3D calculations, while at lower bombarding energies one does obtain fusion in 2D model R1.⁶

Another comparison^{11,18} was for $^{40}\text{Ca}+^{40}\text{Ca}$ at $E_{\text{lab}} = 278$ MeV. Again at this energy there is fusion for 3D but not for 2D. Yet we know that at lower energies one does see fusion for $^{40}\text{Ca}+^{40}\text{Ca}$ using the rigid clutching 2D model.⁶ Thus, it becomes important to make a detailed comparison between the various axially-symmetric 2D models and the 3D theory for an energy at which one obtains a considerable amount of fusion in 2D.

Also, since axially-symmetric 2D studies of very heavy nuclei are currently being pursued,^{16,17} it is of interest to try to ascertain the probable validity of these 2D models for such reactions. For this purpose, we have chosen to study a regime in which the relative velocity above the Coulomb barrier is the same for $^{40}\text{Ca}+^{40}\text{Ca}$ as it is for a very heavy-ion reaction. For the latter we choose $^{84}\text{Kr}+^{209}\text{Bi}$ at $E_{\text{lab}} = 600$ MeV,²¹ from which we find that the corresponding energy for $^{40}\text{Ca}+^{40}\text{Ca}$ is $E_{\text{lab}} = 192$ MeV. Fortunately, at this energy there is considerable fusion in the axially-symmetric 2D calculations of $^{40}\text{Ca}+^{40}\text{Ca}$.

In Fig. 7 we display the energy loss and deflection function curves for the 2D phase model and the 2D rigid, clutching model R2. We also show isolated points obtained from 3D calculations,¹⁴ for which one observes a large fusion window from $L \approx 10\hbar$ to $L \approx 50\hbar$. For the phase model, there is a narrow fusion window centered about $L \approx 20\hbar$. The rigid clutching model exhibits a wider fusion window, which extends from $L \approx 30\hbar$ to $L \approx 50\hbar$. Together the two 2D fusion windows fairly well span almost the entire 3D window, with the phase model giving fusion at the lower end and the rigid clutching model, from the middle section to the upper part of the 3D window. This agrees with our qualitative understanding of the 2D models observed in the last subsection. For the energy loss graph in Fig. 7 the dot-dashed curve is for prescription R4 (discussed in Sec. II A), and it is seen that this curve is only a few MeV below the 3D points, which is within the numerical uncertainties in the calculations. Notice that, just as in $^{16}\text{O}+^{16}\text{O}$, the phase model seems to break down for the higher L values. For the upper part of the 3D fusion window and in the region above fusion, the rigid clutching model seems superior to the phase model for reproducing the 3D results.

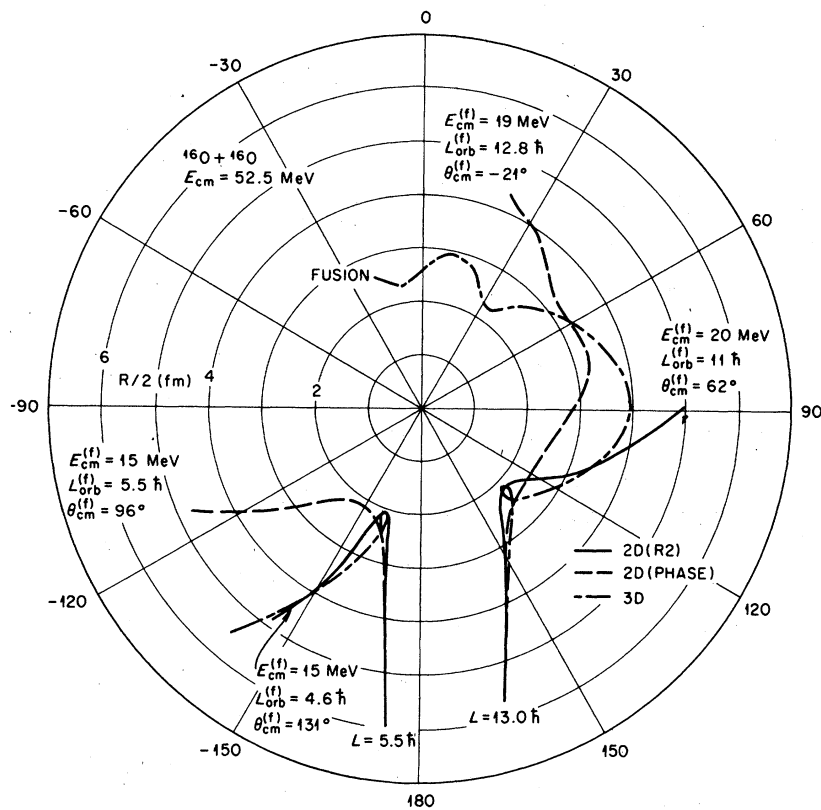


FIG. 5. R - θ trajectories for $^{16}\text{O}+^{16}\text{O}$ at $E_{c.m.} = 52.5$ MeV and for $L = 5.5\hbar$ and $L = 13\hbar$. The full curves are for 2D model R2, the dashed curves are for the 2D phase model, and the dot-dashed curves are from the 3D calculations (Ref. 10). $L_{orb}^{(f)}$ is the final orbital angular momentum.

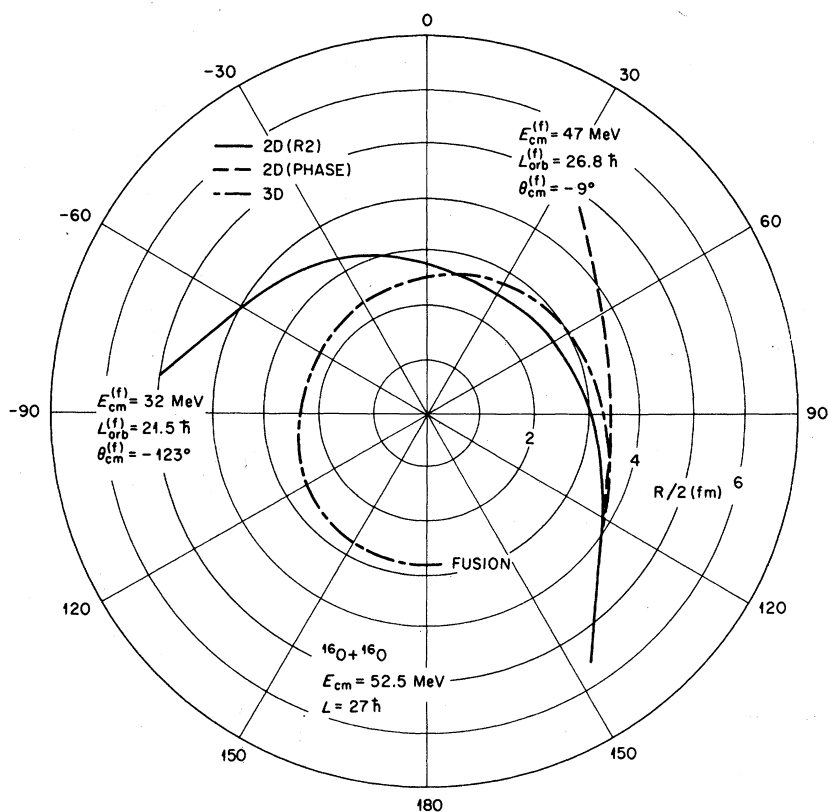


FIG. 6. R - θ trajectories for $^{16}\text{O}+^{16}\text{O}$ at $E_{c.m.} = 52.5$ MeV and $L = 27\hbar$. The notation for the curves is the same as in Fig. 5. $L_{orb}^{(f)}$ is the final orbital angular momentum.

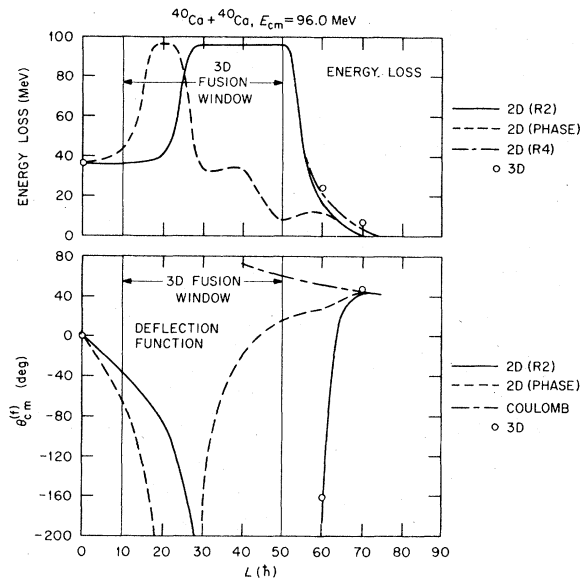


FIG. 7. Energy loss and deflection function curves for $^{40}\text{Ca} + ^{40}\text{Ca}$ at $E_{\text{c.m.}} = 96$ MeV. The full curve is for 2D model R2, the dashed curve is for the 2D phase model, and the circles are the results of the 3D calculation (Ref. 14). The dot-dashed curve for the energy loss graph is for 2D prescription R4. The dot-dashed curve for the deflection function graph is for pure Coulomb scattering.

Finally, it is of interest to compare in detail all of the various axially-symmetric 2D models discussed in Sec. II. In Table II, we present our results for two crucial angular momenta: $L = 60\hbar$ which gives orbiting behavior for all cases and $L = 70\hbar$ which is very close to grazing. The results from the various 2D rigid clutching models, the 2D phase model, and the 3D theory can all be compared. In reproducing the 3D results, it is seen that the phase model and prescription R1 are clearly worse than the remaining 2D models. Prescription R4 gives the best agreement with the 3D results for energy loss, but at $L = 60\hbar$ the deflection angle is much too negative. However, since the angle is changing rapidly in this region, this may not be a serious problem. Also, Table II shows that for prescription R4 the deflection angle becomes less negative if the clutching density ρ_c is increased. Prescriptions R2 and R3 give very similar results, and overall we feel the agreement with 3D is best for these two models.

IV. CONCLUSIONS

Various axially-symmetric 2D TDHF models have been discussed. Four of these are based on the assumption that when the two ions clutch, the moment of inertia is that of a rigid body.^{2,5,7} The

TABLE II. Comparisons of $\theta_{\text{c.m.}}^{(f)}$ and energy loss for $^{40}\text{Ca} + ^{40}\text{Ca}$ at $E_{\text{lab}} = 192$ MeV. The notation 2D, P indicates the 2D phase model (Ref. 12). For the rigid clutching model we use $\rho_c = 0.07 \text{ fm}^{-3}$ unless otherwise indicated, as in the last two $L = 60\hbar$ cases for which the ρ_c values are listed in parentheses.

L/\hbar	Case	$\theta_{\text{c.m.}}^{(f)}$ (degrees)	Energy loss (MeV)
60	3D ¹⁴	-161	24
60	2D, P	-153	12
60	2D, R1	-182	6
60	2D, R2	-175	17
60	2D, R3	-174	19
60	2D, R4	-232	21
60	2D, R4 ($\rho_c = .10$)	-222	24
60	2D, R4 ($\rho_c = .12$)	-213	24
70	3D ¹⁴	45	7
70	2D, P	43	0
70	2D, R1 - 3	42	0
70	2D, R4	42	3

remaining 2D model is a self-consistent phase approximation which results in an irrotational moment of inertia.¹² The results obtained using these different models are compared with each other and with results from an exact 3D TDHF calculation.^{10,14} We have studied $^{16}\text{O} + ^{16}\text{O}$ at $E_{\text{c.m.}} = 52.5$ MeV and $^{40}\text{Ca} + ^{40}\text{Ca}$ at $E_{\text{c.m.}} = 96$ MeV.

We find that 2D seems to agree reasonably well with 3D for L values in the regions both below and above the 3D fusion window. For bombarding energies for which we obtain fusion in 3D but not in 2D, the phase model exhibits orbiting at the lower part of the 3D fusion window while the rigid clutching model displays orbiting at the upper part of the window. Similarly, at lower energies for which we observe fusion in both 2D and 3D, the phase model and the rigid clutching model exhibit fusion for the lower and upper parts, respectively, of the 3D fusion window. Without further investigation of the 3D wave functions, it is not possible to conclude that the 3D moment of inertia is largely irrotational for small impact parameters and is dominated by rigid-body behavior for higher values of L . However, the above results suggest this behavior.

Of all of the 2D models, the rigid clutching prescriptions R2 and R3 seem to give the best overall agreement with 3D for L values at the upper end of the 3D fusion window, for orbiting, and for peripheral scattering. Therefore, we recommend that either R2 or R3 be used in the calculations of very heavy-ion scattering, in which orbiting and peripheral-type behavior are thought to dominate.

ACKNOWLEDGMENTS

We would especially like to thank R. Y. Cusson, S. E. Koonin, and J. W. Negele for a number of

helpful suggestions. We would also like to acknowledge useful discussions with S. J. Krieger, J. A. Maruhn, V. Maruhn-Rezwani, and J. R. Nix.

- †This work was sponsored in part by the Division of Physical Research, U. S. Department of Energy, under Contract No. W-7405-eng-26 with the Union Carbide Corporation, and under Contract No. W-7405-eng-48.
- ¹P. Bonche, S. E. Koonin, and J. W. Negele, Phys. Rev. C 13, 1226 (1976).
- ²S. E. Koonin, Phys. Lett. 61B, 227 (1976).
- ³R. Y. Cusson and J. Maruhn, Phys. Lett. 62B, 134 (1976).
- ⁴R. Y. Cusson, R. K. Smith, and J. A. Maruhn, Phys. Rev. Lett. 36, 1166 (1976).
- ⁵J. A. Maruhn and R. Y. Cusson, Nucl. Phys. A270, 437 (1976).
- ⁶S. E. Koonin, K. T. R. Davies, V. Maruhn-Rezwani, H. Feldmeier, S. J. Krieger, and J. W. Negele, Phys. Rev. C 15, 1359 (1977).
- ⁷V. Maruhn-Rezwani, K. T. R. Davies, and S. E. Koonin, Phys. Lett. 67B, 134 (1977).
- ⁸J. W. Negele, S. E. Koonin, P. Möller, J. R. Nix, and A. J. Sierk, Phys. Rev. C 17, 1098 (1978).
- ⁹R. Y. Cusson and J. A. Maruhn, to be published.
- ¹⁰H. Flocard, S. E. Koonin, and M. S. Weiss, Phys. Rev. C 17, 1682 (1978).

- ¹¹P. Bonche, B. Grammaticos, and S. Koonin, Phys. Rev. C 17, 1700 (1978).
- ¹²H. T. Feldmeier, Report No. ORNL/TM-6053, 1977 (unpublished).
- ¹³K. R. Sandhya Devi and M. R. Strayer, in press, Phys. Lett. B; J. Phys. G 4, L97 (1978).
- ¹⁴S. E. Koonin, B. Flanders, H. Flocard, and M. S. Weiss, Phys. Lett. B 77, 13 (1978).
- ¹⁵M. S. Weiss, Proceedings of the Bléd Conference, 1977 (to be published in Fizika).
- ¹⁶K. T. R. Davies, V. Maruhn-Rezwani, S. E. Koonin, and J. W. Negele, Phys. Rev. Lett. 41, 632 (1978).
- ¹⁷A. K. Dhar and B. S. Nilsson, Report No. NBI-78-4, to be published. Since this 2D study is for a head-on collision of $^{208}\text{Pb} + ^{208}\text{Pb}$, the results should exactly agree with a 3D calculation.
- ¹⁸H. Flocard and M. S. Weiss, Report No. UCRL-80772 [Phys. Rev. C (to be published)].
- ¹⁹M. J. Giannoni, D. Vautherin, M. Veneroni, and D. M. Brink, Phys. Lett. 63B, 8 (1976).
- ²⁰S. E. Koonin, Ph.D. thesis, M.I.T., 1975 (unpublished).
- ²¹K. L. Wolf, J. P. Unik, J. R. Huizenga, J. Birkelund, H. Freiesleben, and V. E. Viola, Phys. Rev. Lett. 33, 1105 (1974).